J Mater Sci (2018) 53:13173–13185

Metals

Influence of microstructure on thermal stability of ultrafine-grained Cu processed by equal channel angular pressing

Ningning Liang[1], Yonghao Zhao[1,*], Y. Li[2], T. Topping[2], Yuntian Zhu[1,3], R. Z. Valiev[4], and E. J. Lavernia[5]

[1] *Nano and Heterogeneous Materials Center, School of Materials Science and Engineering, Nanjing University of Science and Technology, Nanjing 210094, China*
[2] *Department of Chemical Engineering and Materials Science, University of California, Davis, Davis, CA 95616, USA*
[3] *Department of Materials Science and Engineering, North Carolina State University, Raleigh, NC 27695-7919, USA*
[4] *Institute of Physics of Advanced Materials, Ufa State Aviation Technical University, Ufa, Russia 450000*
[5] *Department of Chemical Engineering and Materials Science, University of California, Irvine, Irvine, CA 95616, USA*

Received: 8 March 2018
Accepted: 5 June 2018
Published online: 12 June 2018

ABSTRACT

The well-established enhanced mechanical performance of ultrafine-grained (UFG) materials is often accompanied by poor thermal stability which precludes their use in some applications. To provide fundamental insight into the problem of thermal stability, we studied the microstructure of two different UFG microstructures in Cu: one with lamellar grains and low-angle grain boundaries (GBs) and another with equiaxed grains and high-angle GBs. These distinct microstructures were obtained using equal channel angular pressing (ECAP) for 2 and 16 passes, respectively. Our results show that both microstructures exhibited a similar yield strength, but the material processed using two passes (ECAP-2) exhibited a higher thermal stability when compared to that of ECAP-16. Thermodynamic calculations indicate that the ECAP-2 Cu has a lower stored energy (0.43 J/g) relative to that of the ECAP-16 Cu (0.66 J/g) because the former microstructure has lower GB energy and lower GB volume fraction relative to the latter one. Kinetic analysis revealed that the ECAP-2 Cu has higher activation energy of recrystallization (94 kJ/mol) as compared to that corresponding to the ECAP-16 Cu (72 kJ/mol).

Introduction

Ultrafine-grained (UFG) and nano-structured (NS) materials reportedly exhibit superior properties relative to those of conventional materials, making them attractive for many structural and functional applications [1–3]. For coarse-grained (CG) materials, only a small fraction of atoms are spatially located at or in the immediate vicinity of grain boundaries (GBs). However, UFG materials have a large volume

Address correspondence to E-mail: yhzhao@njust.edu.cn

https://doi.org/10.1007/s10853-018-2548-1

fraction of GBs, leading to more atoms residing near GBs [4, 5]. Comparing with grain interior, the atomic packing at GBs is less dense and more disordered, which increases the configurational and vibrational entropy of the entire system [6] and consequently leads to higher Gibbs energy. This in turn leads to thermal instability of UFG/NS materials [7–10], which leads to dislocation recovery, recrystallization and gain growth at elevated temperatures, or even at low to room temperatures [11–14]. For example, Huang et al. [12] reported self-annealing of high-purity Cu at room temperature processed by high-pressure torsion (HPT). Theoretically, the effective driving force P and velocity V_G of thermally driven grain growth on GBs is given by Abdeljawad and Foiles [5, 15] and Darling et al. [5, 15]:

$$P = \gamma_{GB} K \quad (1)$$

$$V_G = MP = M\gamma_{GB} K \quad (2)$$

where K is the local mean curvature, γ_{GB} is the GB energy and M is the GB mobility. For UFG/NS material, high stored enthalpy introduced by dislocation defects as well as high GB curvature K provide a high driving force for grain growth.

In order to improve the thermal stability, alloying elements were usually introduced into pure UFG/NS materials to lower the grain growth kinetics (i.e., M in Eq. 2) and thermodynamic driving force (γ_{GB}) [16]. A reduction in grain growth kinetics can be realized by solute dragging and second-phase pinning of GB [17–19], while the thermodynamic driving force can be reduced by solute or impurity segregation to GBs, which reduces the GB energy [15, 17, 20, 21]. For example, Atwater et al. [17] added 1 at.% Zr to Cu and raised the stability of the nano-grains to about 900 °C, which exceeds 0.85 T_m, the melting temperature for pure Cu.

It is more challenging to stabilize UFG/NS structures of pure metals, but some examples have been reported. Liu et al. [22] reported that 2D nano-laminated structure on top of bulk Ni with low-angle grain boundaries (LAGBs) produced by surface mechanical grinding treatment (SMAT) is much more stable than the corresponding 3D UFG structure, which is attributed to the low excess energy and low mobility of the LAGBs. Nano-Cu with large amount of twin boundaries was also found to have high thermal stability [23, 24]. It is of interest to process UFG metals with both good mechanical properties and high thermal stability.

Equal channel angular pressing (ECAP) is an effective technique to produce UFG metals [25–27]. Dalla Torre et al. [27] found that ECAP processing for 1–2 passes significantly improve the strength of pure Cu, while greater number of passes, especially after 8, have limited effect on strength [27, 28]. Higher ECAP passes or higher strain can be used to improve ductility, as reported in [29]. However, the total elongation to failure improved only from 8.6 to 10.0% when the number of ECAP passes increased from 2 to 16 [27]. With more ECAP passes, dislocation density is expected reduced [27], which makes UFG structure more stable. On the other hand, more high-angle GB (HAGB) is also expected with more processing strain [30], which has higher mobility and lower activation energy for recrystallization than LAGB and therefore makes the UFG structure less stable [25, 31, 32].

It is of interest to investigate the different UFG structures produced by ECAP on the thermal stability. In this work, we systematically studied the thermal stability of bulk pure Cu processed by ECAP with 2 passes and 16 passes, which are hereafter referred to as ECAP-2 and ECAP-16 samples, respectively. The ECAP-2 sample has elongated grains with LAGBs, while the ECAP-16 sample has equiaxed grains with HAGBs. Both thermodynamic and kinetic factors are considered in the experiments, data analysis and discussion. The discontinuous annealing process and the mechanisms of thermal stability were also studied.

Experimental procedures

Polycrystalline Cu with a purity of 99.99% was chosen as starting material. ECAP samples of $20 \times 20 \times 80$ mm^3 were annealed at 500 °C for 120 min. to produce a recrystallized microstructure with an average grain size of 55 μm (Fig. 1a). ECAP processing was carried out at room temperature using a die with an internal channel angle of 90° and the outer curvature angle is 45°. Two and 16 passes were employed through route B_C, in which the sample was rotated clockwise by 90° between adjacent passes. More details can be found in [33, 34].

Thermal stability was examined by isothermal and isochronal annealing. Isothermal annealing was performed at 200 °C in silicone oil for different durations

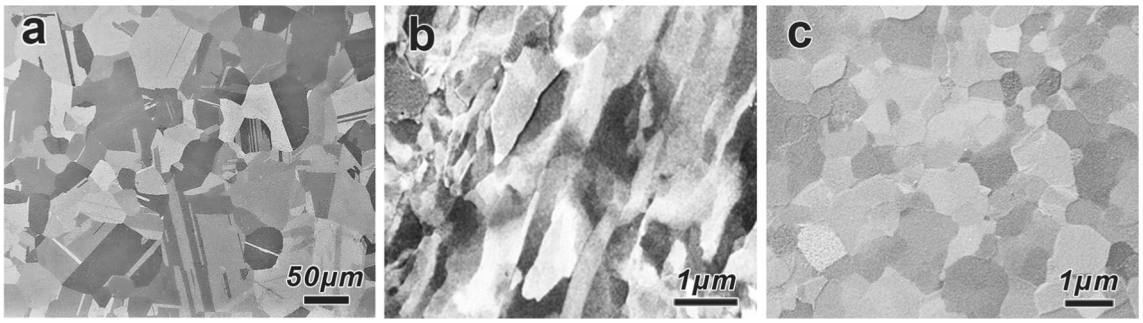

Figure 1 SEM images of: **a** annealed Cu sample with an average grain size of 55 μm, **b** ECAP-2 Cu with elongated subgrain structure and **c** ECAP-16 Cu with a UFG equiaxed grain structure.

from 5 to 480 min. Isochronal annealing was performed in argon protective atmosphere for 30 min at temperatures from 150 to 350 °C followed by air cooling. Vickers microhardness was measured to evaluate the softening during annealing with a load of 2.94 N and a loading time of 10 s. Each value was averaged over at least 15 measurements. Quasi-static uniaxial tensile tests were conducted at room temperature on an Instron 8801 universal testing machine (UTM) with a strain rate of 1×10^{-3} s^{-1}. Flat dog-bone-shaped tensile specimens were sectioned by electrical discharge machining (EDM) from the central regions of the UFG Cu square bars along the longitudinal direction. The gauge dimension is $2 \times 1 \times 10$ mm^3, and sample surface was polished with 1-μm diamond suspension before tests. Three tensile specimens were tested for each annealing condition to get error bars.

The microstructure was characterized by scanning electron microscopy (SEM) and electron backscattered diffraction (EBSD). Samples sectioned from the plane perpendicular to the longitudinal direction of the ECAP-processed bar were ground and electropolished using 2.1 V alternating current in 85% H_3PO_4 + 15% deionized water. Scanning was completed using Zeiss Auriga crossbeam microscope operated at 5 kV and equipped Oxford EBSD detector working at 20 kV with a step size of 0.03 μm. Microstructure was also characterized in a Philips CM12 transmission electron microscope (TEM) operated at 100 kV. TEM specimens were prepared by first mechanically grinding the samples to a thickness of about 50–70 μm, then dimpling to a thickness of about 10 μm and finally ion milling to a thickness of electron transparency using a Gatan Precision Ion Milling System with an Ar^+ accelerating voltage of 4 kV and below 35 °C.

Results

As deformed microstructures

An elongated subgrain structure was formed after ECAP processing for 2 passes inside an initial CG grain (Fig. 1b). The fuzzy subgrain boundaries indicate LAGBs, and the gradient, non-uniform contrast indicates high density of dislocations, which are not uniformly distributed and likely entangled [35]. Average width of the elongated subgrains was measured as about 230 nm, which is consistent with previous reports [27, 33]. After 16 ECAP passes, the microstructure was refined to equiaxed grains with an average diameter of about 270 nm as presented in Fig. 1c. Sharp GBs and clean grain interior manifest the occurrence of dynamic recovery and dynamic recrystallization during the severe plastic deformation [26, 27].

Figure 2 displays the EBSD results of as-ECAP-processed Cu. As shown in Fig. 2a, b as scanned different large regions, initial CG grains were deformed where elongated subgrain structure was formed in the deformed grains. Figure 2c, d is representative small area, one of the scanning regions with accurate step size and resolution, which was used to give the impression of grain structure. For ECAP-2, there exist abundant LAGBs (gray lines) in the elongated grains (Fig. 2b, c). Some small irregular subgrains with unclosed boundary also exist in Fig. 2b, c, indicating the boundaries with misorientation angle less than 2°. Figure 2d shows that the ECAP-16 sample is mostly composed of equiaxed clean grains surrounded by HAGBs (black lines). Moreover, the interiors of grains are relatively clean, possibly due to dynamic recovery and recrystallization during ECAP process.

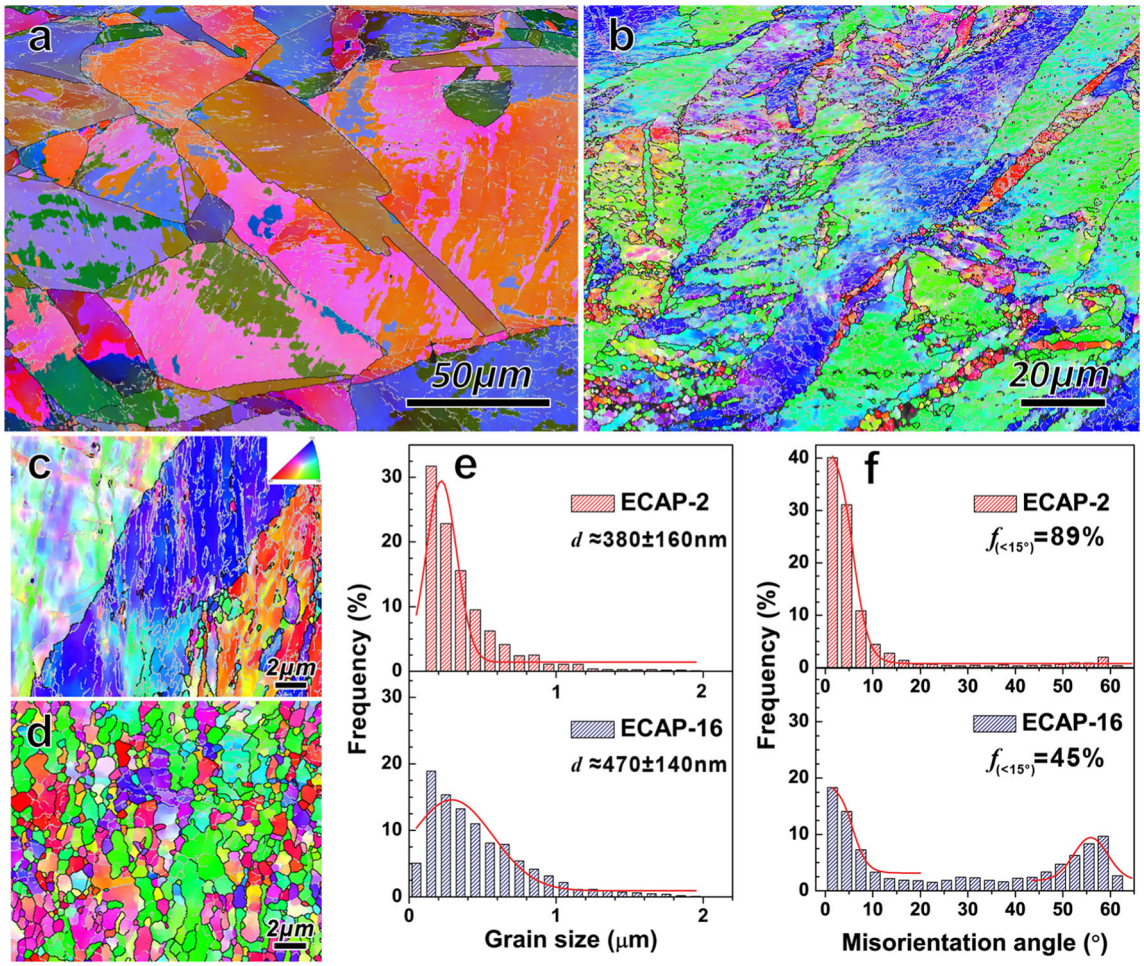

Figure 2 **a**, **b** are the orientation imaging microscopy (OIM) images of as-processed ECAP-2 with different scanning areas. **c**, **d** are magnified OIM images of ECAP-2 and ECAP-16 samples, respectively. Black lines indicate boundary misorientation > 15°, and gray lines indicate misorientation between 2° and 15°. The distribution of **e** grain size and **f** misorientation is measured statistically from EBSD data.

Grain size (or lamella thickness) distribution (Fig. 2e) indicates that both the ECAP-2 and ECAP-16 samples have one size peak, and the average subgrain/grain size is 380 ± 160 and 470 ± 140 nm, respectively. The fractions of small subgrains (< 500 nm) in the ECAP-2 sample are obviously higher than that of small grains in the ECAP-16 sample. It is noted that the average grain size measured by EBSD disagrees with that by SEM data, because EBSD is based on Kikuchi pattern and orientation information, while SEM images cannot distinguish HAGB and LAGB. Misorientation distribution map is exhibited in Fig. 2f. For the ECAP-2 sample, 89% of the boundaries are LAGBs and about 65% of boundaries have misorientation angle below 5° [25]. In contrast, the ECAP-16 sample exhibits a bimodal distribution with one peak appearing at low angles and the other peak at high angles. The fraction of HAGB is 55% [31], which is much higher than that in the ECAP-2 sample (11%).

Microhardness evolutions

The evaluation of microhardness and yield strength of specimens after isochronal and isothermal annealing is illustrated in Fig. 3. All the hardness (or strength) value versus annealing condition exhibits similar trends of softening with increasing annealing temperature due to dislocation recovery and grain growth. Three decrease stages, slow decrease, quick drop and gradual decrease, typically exist with increasing annealing temperatures and time [25, 36–38]. Recovery is responsible for slow decrease stage, which is caused by dislocation rearrangement

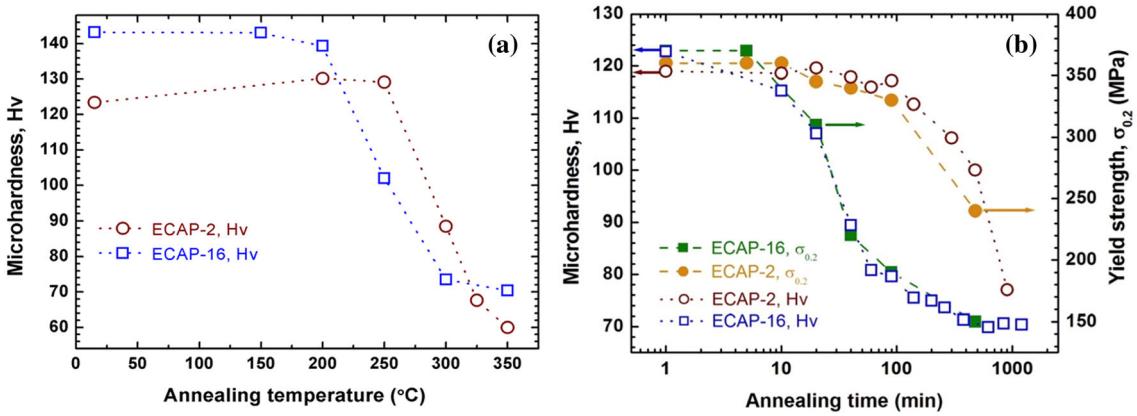

Figure 3 **a** Microhardness evolution of UFG Cu during 30-min isochronal annealing and **b** evolutions of microhardness and yield strength with isothermal annealing time at 200 °C. The tensile tests were conducted at quasi-static tension at 1×10^{-3} s^{-1}. The error of yield strength and hardness is about ± 10 MPa and ± 5, respectively.

and annihilation. The rapid drop stage is caused by recrystallization, which may clean grain interior and produce annealing twins over a short time period or temperature range. This is related to discontinuous recrystallization and grain growth, which will be discussed in a subsequent section. In the last stage, strength gradually decreases due to overall grain growth.

Figure 3 demonstrates that the ECAP-2 sample has higher thermal stability than that corresponding to the ECAP-16 sample. During the 30-min isochronal annealing (Fig. 3a), the ECAP-2 sample started to soften at about 250 °C, which is about 50 °C higher than that of ECAP-16 sample (< 200 °C). The setup temperature of recrystallization was decreased for samples with higher ECAP processing passes which was reported by Cao et al. [31]. The difference for ECAP-2 and 16 is consistent with Cao et al. [31] (215 °C for 1 pass and 169 °C for 16 passes). Similarly, during isothermal annealing at 200 °C the ECAP-2 sample maintained hardness for 90 min, while ECAP-16 sample exhibited a sustained softening from the outset (Fig. 3b). As expected, yield strength variation matches the variation trend of hardness. A slight annealing hardening is also observed for ECAP-2 sample attributing to the dislocation source-limited strengthening where the relaxation of GB as dislocation source occurs after annealing and more force is needed to activate it [39, 40].

Microstructural evolution during annealing

Figure 4 illustrates the microstructural evolution of the ECAP deformed Cu samples during isochronal annealing. Generally, with increasing temperature, recrystallized areas nucleate and grow, leading to the formation of a bimodal grain size distribution [33] (Fig. 4b–e) where new large grains coexist with deformed UFG matrix [25, 36, 41, 42]. As shown in Fig. 4a, the ECAP-2 samples had no change in microstructure when annealed at temperatures up to 200 °C. A few recrystallized grains are observed at 250 °C with grain size about 3.15 μm (Fig. 4b, red circles). The recrystallization of the ECAP-2 sample is almost completed at 325 °C, with some small areas of remaining deformed structure as marked by orange circles in Fig. 4c. In contrast, the ECAP-16 sample started recrystallization at 200 °C (see the red circles in Fig. 4d). At 300 °C, the recrystallization was almost completed (Fig. 4e). These observations again indicate that the ECAP-2 sample is more stable than the ECAP-16 sample.

Figure 5 illustrates the frequency evolution of different GBs during isochronal annealing. As presented in the top row of Fig. 5a, most boundaries remained low angle at 250 °C and below. Even annealing to 300 °C, nearly 80% of boundaries s are identified as LAGBs. In contrast, the bottom row of Fig. 5a indicates that the LAGB structure is rapidly annealed out and converted to HAGBs. The prominent single 60° column for ECAP-16 sample at 300 °C represents the annealing twins. Figure 5b indicates that about 90% boundaries are HAGBs. These observations indicate

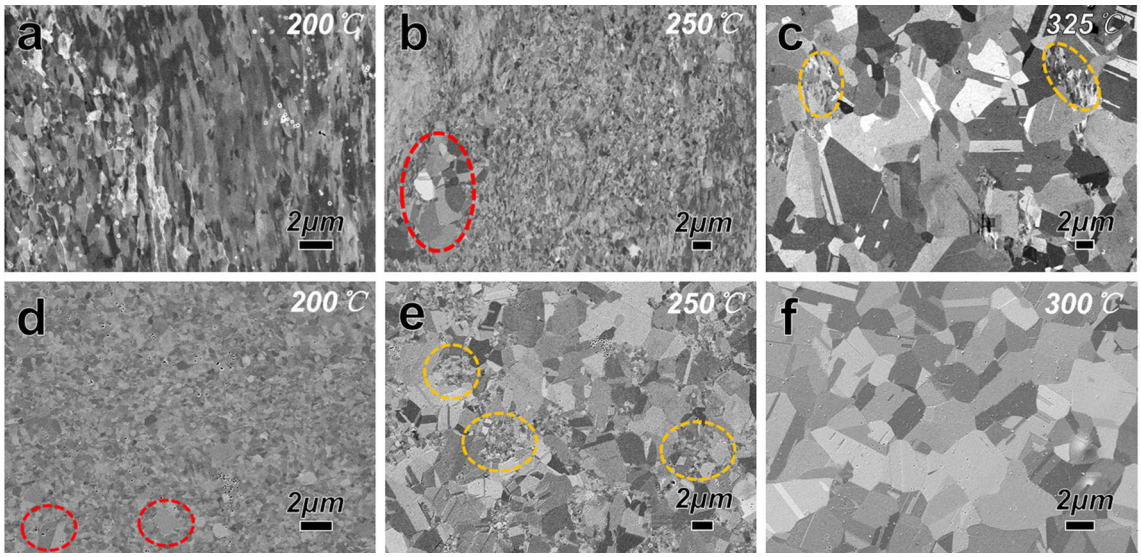

Figure 4 SEM micrographs of microstructures of the ECAP-2 (**a**–**c**) and ECAP-16 (**d**–**f**) samples during 30-min isochronal annealing. Deformed structures and recrystallized grains are marked by orange and red circles, respectively.

that a long recovery process and a delayed recrystallization occurred in the ECAP-2 sample during annealing at temperatures below 0.3 T_m, which is accompanied by nucleation and partial grain growth.

Figure 6 displays TEM microstructures after isothermal annealing. Similar to the microstructures after isochronal annealing, as shown in Fig. 4, recrystallized regions nucleated and expanded gradually with increasing annealing time, which produced a bimodal microstructure distribution (Fig. 6b–e). During annealing at 200 °C, the microstructure of the ECAP-2 samples remained relatively unchanged for 90 min, as shown in Fig. 6a, b, and only recrystallized for a small fraction after 480 min (Fig. 6c). However, the ECAP-16 sample started recrystallization in less than 5 min (Fig. 6d). After annealing for 40 min, about 50% of the area was recrystallized (Fig. 6e). The recrystallization is almost complete after 480 min annealing. These observations again demonstrate higher thermal stability of the ECAP-2 sample.

The evolution of the fraction of recrystallized volume during annealing is summarized in Fig. 7. If we define the recrystallization temperature (T_R) as the temperature at which 50% of the entire area is recrystallized [31] (see the dotted line in Fig. 7a), the T_R of ECAP-2 and ECAP-16 is 295 ± 5 and 240 ± 5 °C, respectively. Therefore, at least 50 °C difference exists between these two samples. To form 50% area fraction of recrystallized grains, the time is postponed from 0.6 h (equiaxed grains, ECAP-16) to 10 h (elongated grain, ECAP-2) for 200 °C isothermal annealing.

Activation energy of recrystallization

To explore the kinetic mechanisms for the observed difference in thermal stabilities of the ECAP-2 and ECAP-16 Cu samples, we estimated the activation energy of recrystallization, using the classical Johnson–Mehl–Avrami–Kolmogorov (JMAK) model [34, 36, 41]. The JMAK equation is expressed by:

$$X_V = 1 - \exp(-Bt^n) \tag{3}$$

where X_V is the volume fraction of recrystallization area, B is a temperature-dependent parameter and n is the JMAK exponent, which is constant. As verified by Ref. [38], the recrystallized area fraction X_A could be used to replace X_V in Eq. (3) for the random distribution and isotropic shape of the recrystallized grains in the present case. Based on the Arrhenius law, B could be represented by:

$$B = B_0 \exp(-Q/RT) \tag{4}$$

where Q is the apparent activation energy of recrystallization, T is absolute annealing temperature and R is gas constant. Then, Eq. (3) can be rewritten as:

$$\ln\left(\ln\frac{1}{1-X_A}\right) - n\ln t = \ln B_0 - \frac{Q}{RT} \tag{5}$$

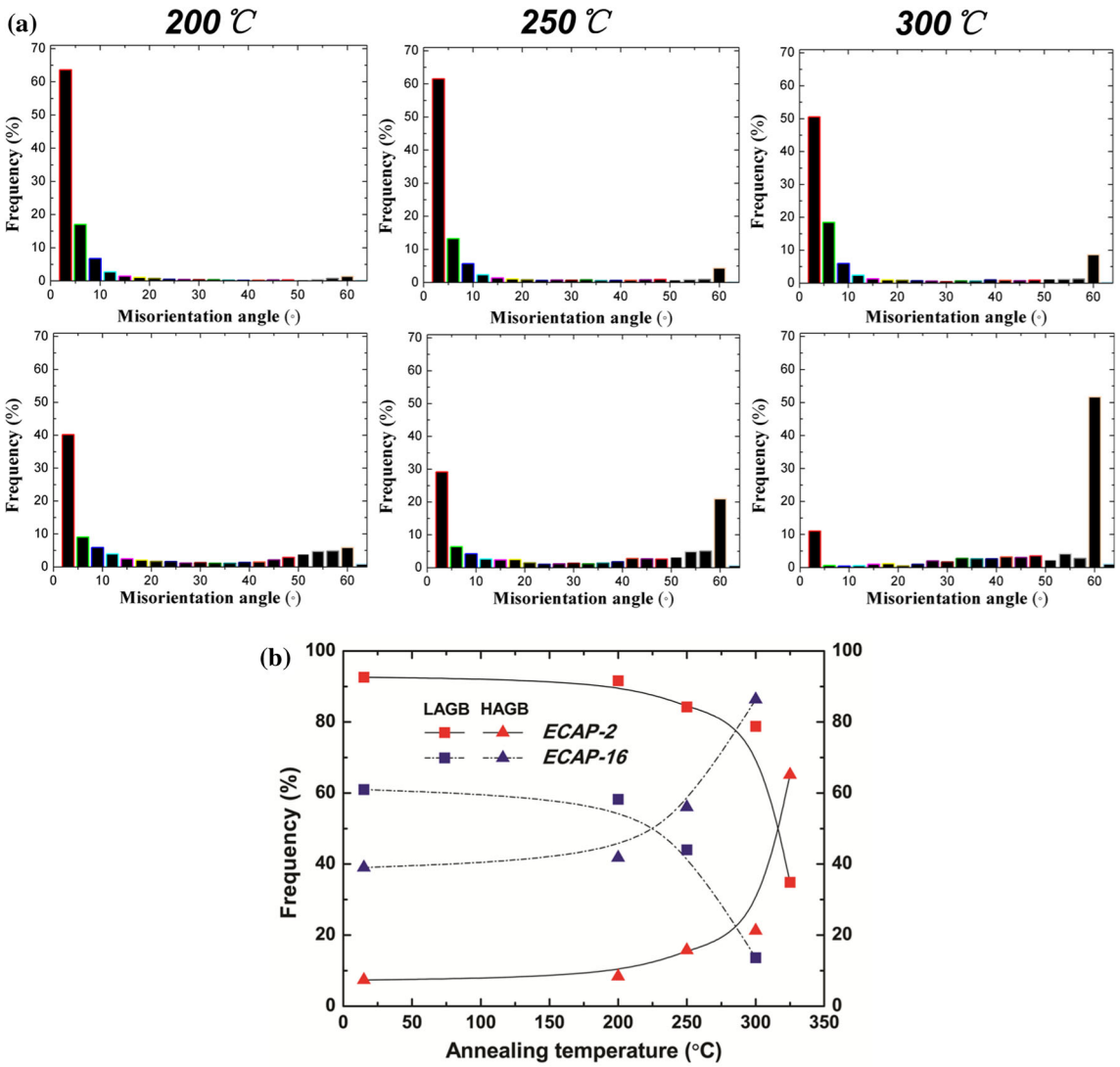

Figure 5 **a** Frequency display of misorientation angle during isochronal annealing for ECAP-2 (top row) and ECAP-16 (bottom row). **b** Frequency evolution of LAGB and HAGB with isochronal annealing temperatures. The frequency data here are original information containing angles below 2° measured by EBSD.

The term $\ln[\ln(1/1 - X_A)]$ for isochronal annealing was plotted against $1/T$ in Fig. 8a. The Q, calculated from the slope of the linear fitting lines to the data using the least square method, is 94 ± 3 kJ/mol and 72 ± 5 kJ/mol for ECAP-2 and ECAP-16 Cu, respectively. The larger Q value of the ECAP-2 Cu compared with that of the ECAP-16 Cu further verifies its higher thermal stability.

Figure 8b shows that the activation energy for recrystallization decreases substantially with increasing number of passes, which is consistent with literature reports [25, 42]. The high activation energy for the ECAP-2 sample was attributed to the large proportion of subgrain structures [42], as also revealed in Figs. 1b and 2a in the present work, while the low Q value for the Cu with high ECAP pass number was due to the higher internal stored energy and higher fraction of HAGBs, which result in a decrease in the energy barrier for nucleation [25, 36, 41].

It was reported that the activation energy for the migration of random HAGBs of Cu is in the range of 104–125 kJ/mol [7, 44], which corresponds to a GB self-diffusion mechanism, while the Q for the migration of LAGBs is measured as 205 kJ/mol [7, 42], close to the Q value of lattice self-diffusion for Cu (197 kJ/mol). The motion of LAGBs is controlled

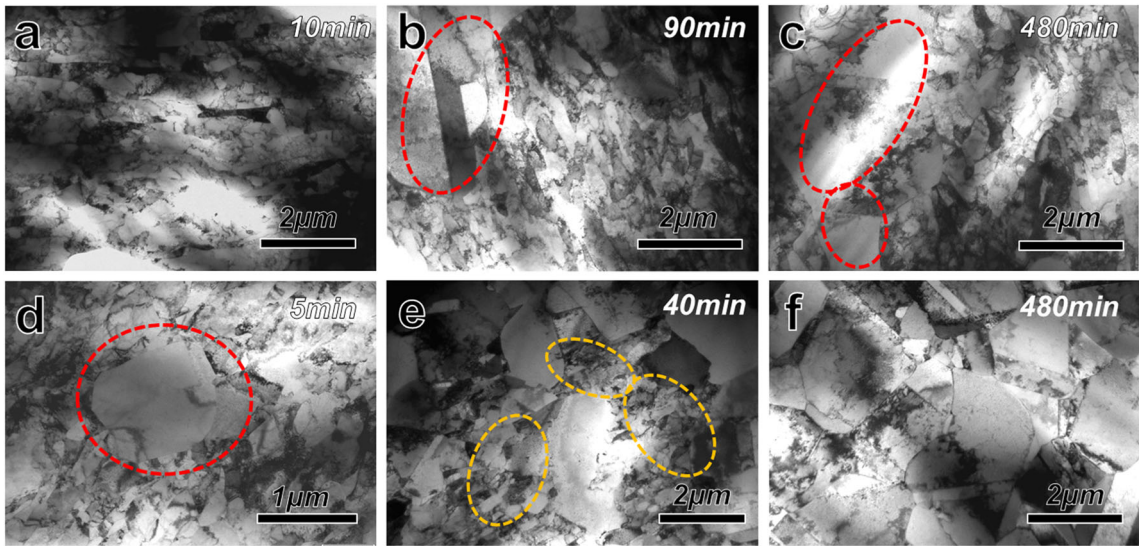

Figure 6 Bright-field TEM images of microstructures of ECAP-2 (**a**–**c**) and ECAP-16 (**d**–**f**) Cu samples during 200 °C isothermal annealing. Deformed structures and recrystallized grains are marked by orange and red circles, respectively.

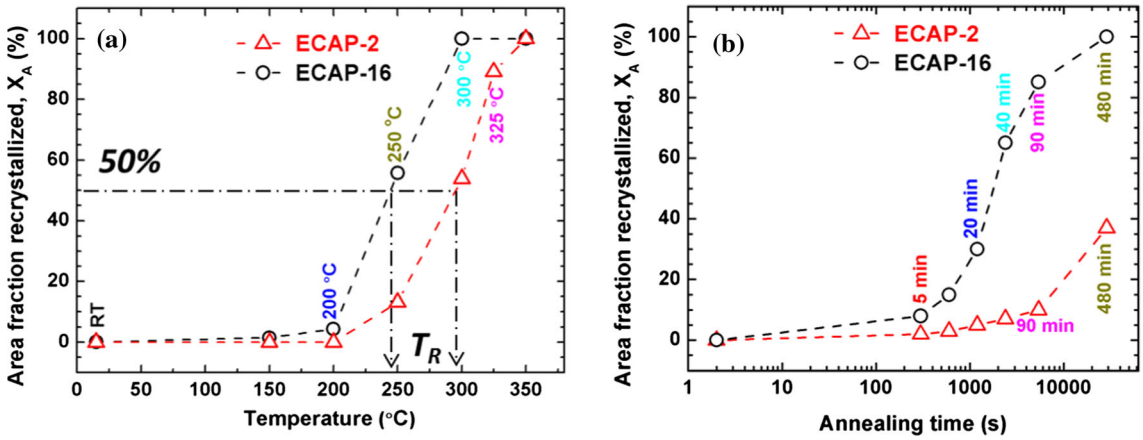

Figure 7 The evolution of recrystallized area fraction of UFG Cu: **a** 30-min isochronal annealing and **b** 200 °C isothermal annealing; data are based on SEM (**a**) and TEM (**b**) observation with at least 20 images for random location.

by dislocation climb via a lattice self-diffusion mechanism. The measured Q values (94 and 72 kJ/mol) in the present work suggest that the recrystallization and grain growth in Cu samples occurred by means of migration of HAGBs.

Stored energy

To further study the thermodynamic origins of the enhanced thermal stability of ECAP-2 Cu, we performed accurate calculation of the stored energy based on the microstructural features (e.g., GBs and dislocations) as measured by TEM and EBSD.

Contribution from GBs

To calculate the contribution to the stored energy from GBs, E_b, one needs to calculate the average GB energy, γ_{GB}, and boundary area per unit volume, S_V [31]. The GB energy, $\gamma(\theta)$, could be calculated by Read–Shockley equation from misorientation across the boundary, θ [31, 42, 45]:

$$\gamma(\theta) = \begin{cases} \gamma_S \dfrac{\theta}{15}\left[1 - \ln\left(\dfrac{\theta}{15}\right)\right], & \theta \le 15^\circ \\ \gamma_S, & \theta > 15^\circ \end{cases} \quad (6)$$

where γ_s is the HAGB energy, equal to 0.625 J/m^2 for Cu [7], and γ_{GB} is obtained by:

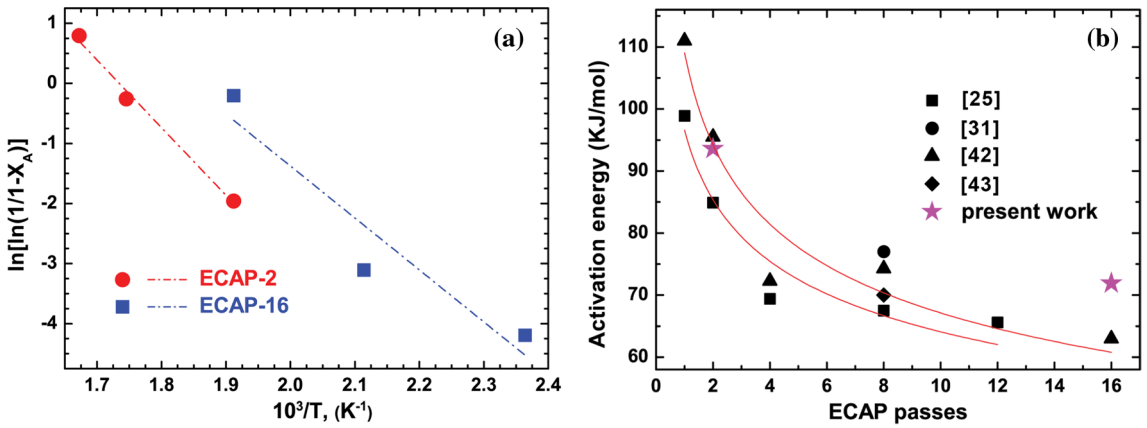

Figure 8 **a** A linear fit of X_A against reciprocal annealing temperature $1/T$ according to Eq. (5). **b** Activation energy of recrystallization kinetics of ECAP deformed Cu with different passes [25, 31, 42, 43].

$$\gamma_{GB} = \sum_{2^\circ}^{63.5^\circ} [\gamma(\theta) f(\theta)] \tag{7}$$

where $f(\theta)$ represents the fraction of a given misorientation θ. The orientation and fraction data are measured by EBSD analysis (Fig. 2f), and the orientation range chosen here is from 2° to 63.5° as angles below 2° are improbable for EBSD scanning. Moreover, as reported by Huang et al. [46] where deformation twins can be found both in ECAP-2 and ECAP-16 samples with considered low density, then they have little effect on average GB energy. The γ_{GB} of ECAP-2 and ECAp-16 is calculated as 0.38 and 0.52 J/m^2, respectively. From the literature, the S_V for equiaxial or cell grain structure could be evaluated as [31, 42]:

$$S_V = \frac{2}{d_{\theta \geq 1^\circ}} \tag{8}$$

where $d_{\theta \geq 1^\circ}$ is the subgrain/grain size. However, the above evaluation was not applicable to the ECAP-2 sample with a lamellar subgrain structure. To calculate S_V of the ECAP-2 sample, we simplified the structural unit as a cuboid with height d_l of 230 nm, length L and width K of about 500 nm [33], as presented in Fig. 9b. Then, S_V is calculated based on:

$$S_V = \frac{d_l L + d_l K + LK}{d_l LK} \tag{9}$$

S_V is then 0.008 nm^{-1} for the ECAP-2 Cu. For ECAP-16 sample with equiaxed grains, as illustrated in Fig. 9c, d, we simplified grains as unit model of cube and hexagonal prism, respectively, with grain size

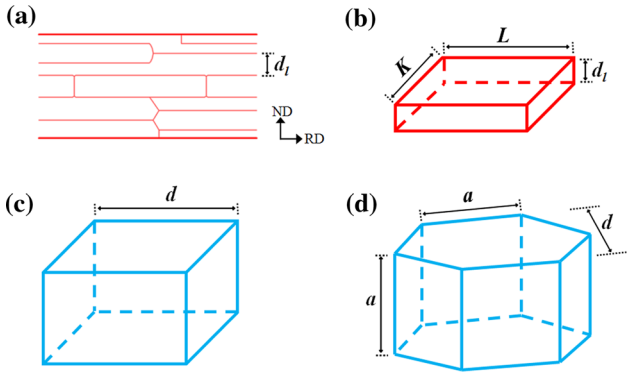

Figure 9 **a**, **b** Simplified lamellar structure as cuboid with length L, width K and height d_l [47]. **c**, **d** Simplified equiaxed grain structure as cube and hexagonal prism, respectively. The grain size is d, and the edge length is "a" in (**d**).

d = 270 nm, as measured from TEM images [33]. The S_V is formulated as:

$$\text{cube,} \quad S_V = \frac{3}{d} \tag{10}$$

$$\text{hexagonal prism} \quad a = \frac{d}{\sqrt{3}}, \quad S_V = \frac{2+\sqrt{3}}{d} \tag{11}$$

Among Eqs. (8), (10) and (11), we choose Eq. (10) to calculate the S_V for ECAP-16 sample which is in reasonable range and consistent with studies [25, 48]. As a result, S_V = 0.011 nm^{-1} for ECAP-16. Then, the boundary contribution to stored energy can be calculated as:

$$E_b = \gamma_{GB} S_V \tag{12}$$

and the calculated values are 0.36 and 0.65 J/g for ECAP-2 and ECAP-16 samples, respectively.

Contribution from dislocations

The stored energy (E_d) for a dislocation density (ρ) is $E_d = \rho E_{dis}$, where E_{dis} is the energy per length unit of dislocation line. But this relationship is appropriate if the dislocations are arranged in such a way that the stress fields of other dislocations are screened, and the energies of the dislocations present in real materials are not wholly represented by such simple considerations. In even moderately worked metals, dislocations are found to intersect each other, and the energy of a dislocation depends on its environment [42]. In most cases, dislocation density at grain interiors contributing to stored energy can be approximatively estimated by Humphreys and Hatherly [7]:

$$E_d = \frac{1}{2}\rho G b^2 \tag{13}$$

where G is the shear modulus (48.3 GPa for Cu) and b is the Burgers vector (2.56×10^{-10} m). As reported in [27], ρ for ECAP-16 was measured to be 0.64×10^{14} m^{-2}, and for ECAP-2, we adopt the ρ of 4.02×10^{14} m^{-2} as measured by Higuera-Cobos et al. [42]. Then, the dislocation-contributed stored energy, E_d, is calculated as 0.07 and 0.011 J/g, respectively. The total stored energy, calculated by $E_S = E_b + E_d$, is 0.43 J/g (ECAP-2) and 0.66 J/g (ECAP-16). This implies that the stored energy increases with increasing ECAP deformation, which agrees with reports from the literature [42]. The higher stored energy in ECAP-16 indicates a higher driving force for recrystallization. This is due to the lower Q and thermal stability measured in ECAP-16 sample. Zi et al. [44] also reported that lower stored energy in cold-rolled Al resulted in higher recrystallization temperature and/or delayed recrystallization.

Discussion

Discontinuous and continuous annealing phenomena

Among various annealing phenomena, recovery, recrystallization and grain growth as the most common processes may occur in a discontinuous and continuous way [7]. Discontinuous processes are characterized by a rapid drop in strength after a narrow annealing temperature interval or time interval and a heterogeneous structural evolution. Typically, discontinuous annealing phenomena include recovery by discontinuous subgrain growth, primary recrystallization and abnormal grain growth, while their borderlines are unclear [7]. In contrast, continuous processes are characterized by a gradual decrease in strength and homogeneous structure coarsening without identifiable nucleation and growth stages. The continuous processes include recovery by subgrain growth, continuous recrystallization and normal grain growth. Large fraction of HAGBs in severely strained material is believed to cause continuous process where the crystallites or grains can readily grow.

In this investigation, heterogeneous structural evolution was observed for ECAP-processed Cu during annealing treatment, and the decreases of hardness and yield strength are in a narrow range for both annealing temperatures and times. These features clearly demonstrate that primary or partial recrystallization occurred during annealing, which are discontinuous phenomena. Similar observations were also reported in [25, 36, 41, 42] for ECAP-processed Cu during subsequent annealing. Koch et al. [16] interpreted the heterogeneous recrystallization based on the facts of the non-uniform distributions of pores and impurities of the ball-milled nano-crystalline samples. For the pure Cu specimens in the current work, the partial primary recrystallization might be caused by the inhomogeneous distributions of deformation strain, which further result in the non-uniform distributions of texture, HAGBs and stored energy, etc. Even for the equiaxed grain structure in the ECAP-16 sample, microstructures are also non-uniform. For example, some nano-grains with a grain size of several tens of nanometers are developed, as observed in Fig. 2d. These small grains are probably recrystallized grains formed during the ECAP process because they are free of dislocations. During the subsequent annealing, these small grains might act as nuclei for recrystallzation and eventually grow.

Thermal stability

From Eqs. (1) to (13), we can see that the thermal stability of NS/UFG materials is determined by thermodynamic and kinetic parameters. The former parameters include the stored energy E_S and GB curvature K, and the latter parameters include GB mobility M and activation energy of recrystallization Q. Both thermodynamic and kinetic parameters are determined by the microstructural characteristics.

Table 1 Lists of grain morphology, fraction of LAGBs, average GB energy γ_{GB}, GB area per unit volume S_V, GB stored energy E_b, dislocation density ρ, dislocation stored energy E_d, total stored energy E_S and activation energy of recrystallization Q, for ECAP-2 and ECAP-16 Cu samples

Samples	Grain morphology	LAGBs (%)	γ_{GB} (J/m^2)	S_V (nm^{-1})	E_b (J/g)	ρ (10^{14} m^{-2})	E_d (J/g)	E_S (J/g)	Q (kJ/mol)
ECAP-2	Lamellar	89	0.38	0.008	0.36	4.02	0.07	0.43	94
ECAP-16	Equiaxed	45	0.52	0.011	0.65	0.64	0.011	0.66	72

Table 1 lists the microstructures and thermodynamic and kinetic parameters for ECAP-2 and ECAP-16 Cu samples.

From Table 1, one can see that the stored energy is primarily originated from the contribution of the GBs (GB energy and area per unit volume), which is one order of magnitude higher than that of dislocations. Due to the high fraction of LAGBs and lamellar grain structure in ECAP-2 Cu, the GB energy and area per unit volume of ECAP-2 Cu (0.38 J/m^2, 0.008 nm^{-1}) are smaller than those of ECAP-16 Cu (0.52 J/m^2, 0.011 nm^{-1}). Moreover, the GB curvature K of lamellar grains in ECAP-2 Cu is much smaller than that of the equiaxed grains in ECAP-16 Cu. Therefore, the thermodynamic driving force for recrystallization of ECAP-2 Cu is smaller than that of ECAP-16 Cu, resulting in its retarded recrystallization.

From the kinetic point of view, the high activation energy of recrystallization of ECAP-2 indicates its large barrier for atom diffusion and boundary migration, i.e., a lower GB mobility M. This can be understood from the different mobility of LAGB and HAGB. LAGBs are found to be much less mobile than HAGBs as the motion of a low-angle boundary involves a coordinated movement of dislocation arrays [36]. For lamellar structured LAGBs, the boundary movement can be normally operated in two dimensions parallel to the lamellar layer, for instance, in the type of Y-junction motion [47, 49]. In the direction perpendicular to the lamella, the migration of lamellar LAGBs is difficult due to geometric constraint (see Fig. 9a) and long boundary line, while the HAGBs, especially surrounding equiaxed grains, can migrate in three dimensions without resistance from geometric constraints. Moreover, it was reported that the GB mobility increases sharply with increasing misorientation, and the mobility of LAGBs could be 10–500 times lower than that of random HAGBs [50].

Conclusions

In this work, we prepared two different Cu samples by ECAP processing for 2 and 16 passes with microstructural characteristics of lamellar grains with LAGBs and equiaxed grains with HAGBs, respectively. The isochronal and isothermal annealing was then performed to evaluate their thermal stability, and EBSD and TEM analyses were carried out to characterize their microstructural evolutions. Thermodynamic calculation of the stored energy and kinetic measurement of the activation energy of recrystallization were carried out to understand the thermal stability. The following conclusions can be made.

1. The EBSD and TEM analyses verified that the recrystallization process of the ECAP-2 Cu was retarded to higher annealing temperature or longer annealing time compared with that of the ECAP-16 Cu.
2. The stored energy of the ECAP-2 Cu is calculated to be smaller than that of the ECAP-16 Cu due to its low GB energy of LAGBs and low boundary area per unit volume. The activation energy for recrystallization of the ECAP-2 Cu is measured to be larger than that of the ECAP-16 due to the low mobility of the LAGBs.
3. With close strength properties and better thermal stability, the elongated microstructure by ECAP-2 for two passes has some advantage in terms of processing cost and engineering application.

Acknowledgements

The authors would like to acknowledge financial supports from the National Key R&D Program of China (Grant No. 2017YFA0204403), the National Natural Science Foundation of China (51225102 and

2012CB932203) and the Jiangsu Key Laboratory of Advanced Micro&Nano Materials and Technologies. EJL would like to acknowledge the support from the US Army Research Office (ARO W911NF-16-1-0269). EBSD and SEM experiments were performed at the Materials Characterization and Research Center of Nanjing University of Science and Technology.

Compliance with ethical standards

Conflict of interest The authors declare that the contents have no conflict of interest.

References

[1] Meyers MA, Mishra A, Benson DJ (2006) Mechanical properties of nanocrystalline materials. Prog Mater Sci 51:427–556

[2] Zeng LF, Gao R, Fang QF, Wang XP, Xie ZM, Miao S (2016) High strength and thermal stability of bulk Cu/Ta nanolamellar multilayers fabricated by cross accumulative roll bonding. Acta Mater 110:341–351

[3] Zhao YH, Zhu YT, Lavernia EJ (2010) Strategies for improving tensile ductility of bulk nanostructured materials. Adv Eng Mater 12:769–777

[4] Millett PC, Selvam RP, Saxena A (2006) Molecular dynamics simulations of grain size stabilization in nanocrystalline materials by addition of dopants. Acta Mater 54:297–298

[5] Abdeljawad F, Foiles SM (2015) Stabilization of nanocrystalline alloys via grain boundary segregation: a diffuse interface model. Acta Mater 101:159–171

[6] Song XY, Zhang JX, Li LM, Yang KY, Liu GQ (2006) Correlation of thermodynamics and grain growth kinetics in nanocrystalline metals. Acta Mater 54:5541–5550

[7] Humphreys FJ, Hatherly M (2004) Recrystallization and related annealing phenomena, 2nd edn. Pergamon Press, Oxford

[8] Koch CC (2006) Nanostructured materials: processing, properties and applications. William Andrew, Norwich

[9] Andrievski RA (2003) Review stability of nanostructured materials. J Mater Sci 38:1367–1874. https://doi.org/10.1023/A:1022988706296

[10] Oh-ishi K, Horita Z, Smith DJ, Valiev RZ, Nemoto M, Langdon TG (1999) Fabrication and thermal stability of a nanocrystalline Ni–Al–Cr alloy: comparison with pure Cu and Ni. J Mater Res 14:4200–4207

[11] Gertsman VY, Birringer R (1994) On the room-temperature grain growth in nanocrystalline copper. Scr Metall Mater 30:577–581

[12] Huang Y, Sabbaghianrad S, Almazrouee AI, Al-Fadhalah KJ, Alhajeri SN, Langdon TG (2016) The significance of self-annealing at room temperature in high purity copper processed by high-pressure torsion. Mater Sci Eng A 656:55–66

[13] Ames M, Markmann J, Karos R, Michels A, Tschöpe A, Birringer R (2008) Unraveling the nature of room temperature grain growth in nanocrystalline materials. Acta Mater 56:4255–4266

[14] Lu L, Tao NR, Wang L, Ding B, Lu K (2001) Grain growth and strain release in nanocrystalline copper. J Appl Phys 89:6408–6414

[15] Darling KA, VanLeeuwen BK, Koch CC, Scattergoodb RO (2010) Thermal stability of nanocrystalline Fe–Zr alloys. Mater Sci Eng A 527:3572–3580

[16] Koch CC, Scattergood RO, Darling KA (2008) Stabilization of nanocrystalline grain sizes by solute additions. J Mater Sci 43:7264–7272. https://doi.org/10.1007/s10853-008-2870-0

[17] Atwater MA, Scattergood RO, Koch CC (2013) The stabilization of nanocrystalline copper by zirconium. Mater Sci Eng A 559:250–256

[18] Darling KA, Kecskes LJ, Atwater M, Semones J, Scattergood RO, Koch CC (2013) Thermal stability of nanocrystalline nickel with yttrium additions. J Mater Res 28:1813–1818

[19] Klemm R, Thiele E, Holste C, Eckert J, Schell N (2002) Thermal stability of grain structure and defects in submicrocrystalline and nanocrystalline nickel. Scr Mater 46:685–690

[20] Chauhan M, Mohamed FA (2006) Investigation of low temperature thermal stability in bulk nanocrystalline Ni. Mater Sci Eng A 427:7–15

[21] Tao JM, Zhu XK, Scattergood RO, Koch CC (2013) The thermal stability of high-energy ball-milled nanostructured Cu. Mater Des 50:22–26

[22] Liu XC, Zhang HW, Lu K (2013) Strain-induced ultrahard and ultrastable nanolaminated structure in nickel. Science 342:337–340

[23] Saldana C, Murthy TG, Shankar MR, Stach EA, Chandrasekar S (2009) Stabilizing nanostructured materials by coherent nanotwins and their grain boundary triple junction drag. Appl Phys Lett 94:021910

[24] Zhang X, Misra A, Wang H, Swadener JG, Lima AL, Hundley MF, Hoagland RG (2005) Thermal stability of sputter-deposited 330 austenitic stainless-steel thin films with nanoscale growth twins. Appl Phys Lett 87:233116

[25] Molodova X, Gottstein G, Winning M, Hellmig RJ (2007) Thermal stability of ECAP processed pure copper. Mater Sci Eng A 460–461:204–213

[26] Valiev RZ, Langdon TG (2006) Principles of equal-channel angular pressing as a processing tool for grain refinement. Prog Mater Sci 51:881–981

[27] Dalla Torre F, Lapovok R, Sandlin J, Thomson PF, Davies CHJ, Pereloma EV (2004) Microstructures and properties of copper processed by equal channel angular extrusion for 1–16 passes. Acta Mater 52:4819–4832

[28] Mishra A, Kad BK, Gregori F, Meyers MA (2007) Microstructural evolution in copper subjected to severe plastic deformation: experiments and analysis. Acta Mater 55:13–28

[29] Valiev RZ, Alexandrov IV, Zhu YT, Lowe TC (2002) Paradox of strength and ductility in metals processed by severe plastic deformation. J Mater Res 17:5–8

[30] Zhao YH, Bingert JF, Zhu YT, Liao XZ, Valiev RZ, Horita Z, Langdon TG, Zhou YZ, Lavernia EJ (2008) Tougher ultrafine grain Cu via high-angle grain boundaries and low dislocation density. Appl Phys Lett 92:081902

[31] Cao WQ, Gu CF, Pereloma EV, Davies CHJ (2008) Stored energy, vacancies and thermal stability of ultra-fine grained copper. Mater Sci Eng A 492:74–79

[32] Haslam AJ, Phillpot SR, Wolf D, Moldovan D, Gleiter H (2001) Mechanisms of grain growth in nanocrystalline fcc metals by molecular-dynamics simulation. Mater Sci Eng A 318:293–312

[33] Liang NN, Zhao YH, Wang JT, Zhu YT (2017) Effect of grain structure on Charpy impact behavior of copper. Sci Rep 7:44783

[34] Zhao YH, Topping T, Li Y, Lavernia EJ (2011) Strength and ductility of bimodal Cu. Adv Eng Mater 13:865–871

[35] Huang JY, Zhu YT, Jiang H, Lowe TC (2001) Microstructures and dislocation configurations in nanostructured Cu processed by repetitive corrugation and straightening. Acta Mater 49:1497–1505

[36] Wang YL, Lapovok R, Wang JT, Qi YS, Estrin Y (2015) Thermal behavior of copper processed by ECAP with and without back pressure. Mater Sci Eng A 628:21–29

[37] Sun PL, Zhao YH, Tseng TY, Su JR, Lavernia EJ (2014) Annealing behavior of ultrafine-grained aluminium. Philos Mag 94:476–491

[38] Zi A, Stulikova I, Smola B (2010) Response of aluminum processed by extrusion preceded ECAP to isochronal annealing. Mater Sci Eng A 527:1469–1472

[39] Huang XX, Hansen N, Tsuji N (2006) Hardening by annealing and softening by deformation in nanostructured metals. Science 312:249–251

[40] Zhang XY, Liu Q, Wu XL, Zhu AW (2008) Work softening and annealing hardening of deformed nanocrystalline nickel. Appl Phys Lett 93:261907

[41] Amouyal Y, Divinski SV, Klinger L, Rabkin E (2008) Grain boundary diffusion and recrystallization in ultrafine grain copper produced by equal channel angular pressing. Acta Mater 56:5500–5513

[42] Higuera-Cobos OF, Cabrera JM (2013) Mechanical, microstructural and electrical evolution of commercially pure copper processed by equal channel angular extrusion. Mater Sci Eng A 571:103–114

[43] Blum W, Li YJ, Durst K (2009) Stability of ultrafine-grained Cu to subgrain coarsening and recrystallization in annealing and deformation at elevated temperatures. Acta Mater 57:5207–5217

[44] Zi A, Stulikova I, Smola B, Riehemann W (2009) Recovery and recrystallization behavior of aluminum processed by extrusion-preceded equal channel angular pressing. Int J Mater Res 100:6

[45] Gazder AA, Araiza MS, Jonas JJ, Pereloma EV (2011) Evolution of recrystallization texture in a 0.78 wt% Cr extra-low-carbon steel after warm and cold rolling. Acta Mater 59:4847–4865

[46] Huang CX, Wang K, Wu SD, Zhang ZF, Li GY, Li SX (2006) Deformation twinning in polycrystalline copper at room temperature and low strain rate. Acta Mater 54:655–665

[47] Yu TB, Hansen N, Huang XX (2011) Recovery by triple junction motion in aluminium deformed to ultrahigh strains. Proc R Soc A 467:3039–3065

[48] Zhang Y, Wang JT, Cheng C, Liu JQ (2008) Stored energy and recrystallization temperature in high purity copper after equal channel angular pressing. J Mater Sci 43:7326–7330. https://doi.org/10.1007/s10853-008-2903-8

[49] Yu TB, Hughes DA, Hansen N, Huang XX (2015) In situ observation of triple junction motion during recovery of heavily deformed aluminum. Acta Mater 86:269–278

[50] Huang Y, Humphreys FJ (2000) Subgrain growth and low angle boundary mobility in aluminium crystals of orientation {110} <001>. Acta Mater 48:2017–2030